

A 4500 year record of palaeomagnetic secular variation and relative palaeointensity from the Tyrrhenian Sea



PONTUS LURCOCK^{1*}, FABIO FLORINDO^{1,2}, SERGIO BONOMO³, ANTONIO CASCELLA⁴, FEDERICO DI RITA⁵, LUCIANA FERRARO⁶, DONATELLA DOMENICA INSINGA⁶, DONATELLA MAGRI⁵, GIULIA MARGARITELLI⁷, NICOLA PELOSI⁶, PAOLA PETROSINO⁸, MATTIA VALLEFUOCO⁶, CLAUDIA COSENTINO⁹ & FABRIZIO LIRER⁶

¹*Istituto Nazionale di Geofisica e Vulcanologia, Via di Vigna Murata 605, 00143 Roma, Italy*

²*Institute for Climate Change Solutions, via Sorchio, 61040-Frontone, Pesaro e Urbino, Italy*

³*Istituto di Studi sul Mediterraneo (ISMED), CNR, Via Cardinale Guglielmo Sanfelice, 8, 80134 Napoli, Italy*

⁴*Istituto Nazionale di Geofisica e Vulcanologia, Via della Faggiola 32, 52126 Pisa, Italy*

⁵*Dipartimento di Biologia Ambientale, Sapienza Università di Roma, Piazzale Aldo Moro 5, 00185 Roma, Italy*

⁶*Istituto di Scienze Marine (ISMAR), Consiglio Nazionale delle Ricerche, Calata Porta di Massa, Interno Porto di Napoli, 80133 Napoli, Italy*

⁷*Istituto di Ricerca per la Protezione Idrogeologica (IRPI), Consiglio Nazionale delle Ricerche, via Madonna Alta 126, 06128, Perugia, Italy*

⁸*DiSTAR – Dipartimento di Scienze della Terra, dell’Ambiente e delle Risorse, Università degli Studi di Napoli Federico II, Complesso di Monte Sant’Angelo (Edificio L), Via Cinthia, 21, 80126 Napoli, Italy*

⁹*Dipartimento di Scienze della Terra e del Mare (DiSTEIM), Università di Palermo, Via Archirafi, 22, Palermo, Italy*

PL, 0000-0001-6994-071X; FF, 0000-0002-6058-9748;
SB, 0000-0001-7077-494X; AC, 0000-0002-8255-3244;
FDR, 0000-0002-3065-8474; LF, 0000-0002-6491-2274;
DDI, 0000-0002-2147-0146; DM, 0000-0001-7254-593X;
GM, 0000-0003-3289-0557; NP, 0000-0002-1751-3844;
PP, 0000-0002-5506-8753; MV, 0000-0003-2822-1764;
CC, 0000-0002-9817-5030; FL, 0000-0003-4938-3252

*Correspondence: pont@talvi.net

Abstract: A marine sediment core from the western Mediterranean provides a new high-resolution 4500 year record of palaeomagnetic secular variation and relative palaeointensity. In 2013, the 7.1 m C5 core was recovered from the Tyrrhenian Sea as part of the NextData climate data project. The coring site, 15 km offshore from the Volturno river mouth, is well located to record combined marine and terrestrial palaeoclimatic influences, and the fine-grained, rapidly deposited sediments are effective palaeomagnetic recorders. We investigate the palaeomagnetic field direction and strength recorded in the core, which provide a valuable high-resolution record of Holocene geomagnetic variation in the area. Using rock magnetic techniques, we constrain the

From: TEMA, E., DI CHIARA, A. & HERRERO-BERVERA, E. (eds) 2020. *Geomagnetic Field Variations in the Past: New Data, Applications and Recent Advances*. Geological Society, London, Special Publications, **497**, 159–178.

First published online July 27, 2020, <https://doi.org/10.1144/SP497-2019-255>

© 2020 The Author(s). Published by The Geological Society of London. All rights reserved.

For permissions: <http://www.geolsoc.org.uk/permissions>. Publishing disclaimer: www.geolsoc.org.uk/pub_ethics

magnetic mineralogy of the studied sediments and confirm their suitability for palaeomagnetic analysis. Palaeomagnetic declination and inclination records were determined by stepwise alternating-field demagnetization, and relative palaeointensity estimates were obtained based on normalization to anhysteretic and isothermal remanent magnetization and to magnetic susceptibility. The age of the core is well constrained with a tephra and biostratigraphic age model, and its magnetic records are compared with relevant core and model data for the region, demonstrating that our record is compatible with previous results from the area. An automated curve matching approach is applied to assess the compatibility of our data with the existing secular variation path for the Mediterranean area.

Supplementary material: The code and data used to produce the results in this paper are available online at <https://doi.org/10.5281/zenodo.1158709>

The magnetic field of the Earth varies significantly and continuously on timescales ranging from milliseconds to centuries (secular variations) and to millions of years. Investigation of palaeomagnetic secular variation (PSV) and longer-term geomagnetic variations through the Earth's history continues to be important for a number of reasons: to improve our understanding of hydrodynamic processes in the Earth's core (e.g. Caricchi *et al.* 2020); to date geological and archaeological materials by matching their magnetic record to reference data and models, and to add to the reference datasets to refine the models (e.g. Lund *et al.* 2020); and to constrain past production rates of cosmogenic radionuclides (e.g. ^{14}C and ^{10}Be) (e.g. Channell *et al.* 2018; Goehring *et al.* 2018), which in turn also helps to date samples. Understanding core–mantle boundary processes requires investigation of both short- and long-term geomagnetic variations, while dating of archaeological materials can be carried out with PSV studies, and dating of older geological material (such as deep-ocean sediments) relates to magnetic processes on timescales of thousands to millions of years.

There are various ways to investigate PSV, each with its own advantages and disadvantages: instrumental records (e.g. Hernandez-Quintero *et al.* 2020) are generally accurate but offer restricted temporal and spatial coverage, with very little data available before 1590; archaeological artefacts (e.g. Turner *et al.* 2020) are only available for times and sites that hosted human settlements; and lava-flow records (e.g. Sánchez-Moreno *et al.* 2020) extend much further into the geological past but only provide spot measurements for single ages and locations. Sediment archives have great potential as recorders of PSV, because they can provide extended, continuous records through long time periods, with ages spanning the Holocene to the Proterozoic, at a huge number of locations worldwide (e.g. Kodama 2012; Panovska *et al.* 2019). One significant limitation of sedimentary archives is that, using current analysis techniques, they can only provide relative, not absolute, palaeointensity records but, for many applications (e.g. dating by curve matching), absolute palaeointensities are not necessary.

In January 2013, as part of the NextData project (<http://www.nextdataproject.it/>), 50 m of late Quaternary sediment were recovered from Tyrrhenian Sea sites near the mouth of the Volturno River in southern Italy (Ferraro *et al.* 2013). The C5 core was one of the cores recovered during this expedition; it, and a short core taken at the same site, have already been studied to investigate climate oscillations over the last five millennia (Bonomo *et al.* 2016; Margaritelli *et al.* 2016; Di Rita *et al.* 2018). In this paper, we present detailed records of PSV (declination and inclination) and relative palaeointensity (RPI), dated by the tephra and biostratigraphic age model of Margaritelli *et al.* (2016), and we compare the results with existing regional records and models.

Site location and core lithology

The C5 coring site is located at latitude $40^{\circ} 58' 24.95''$ N, longitude $13^{\circ} 47' 02.51''$ E on the continental shelf of the Gulf of Gaeta (central-eastern Tyrrhenian Sea) (Fig. 1). The seafloor in this area is presently under the influence of a cyclonic Tyrrhenian Sea circulation which interacts with the intermediate (from 10 to 100 m depth) water layers (Bonomo *et al.* 2014).

The Gulf of Gaeta is also strongly influenced by the two longest rivers of southern Italy, the Volturno (175 km) and the Garigliano (38 km), with estimated mean discharges of 80 and $120 \text{ m}^3 \text{ s}^{-1}$, respectively (Iermano *et al.* 2012). Catchment basins are of the order of 5000 km^2 , and contain mainly Cretaceous, Paleogene and Neogene sedimentary rocks and recent volcanic deposits (Bonardi *et al.* 1988). The location of the coring site subjects it to rapid deposition of fine-grained material with high terrigenous content in a low-energy environment, providing promising conditions for palaeomagnetic work.

The lithology of the C5 core is fairly uniform and dominated by light-grey fine-grained hemipelagic sediments interlayered by tephra horizons attributable to nearby eruptions from Vesuvius, Ischia and the Phlegraean fields (Margaritelli *et al.* 2016).

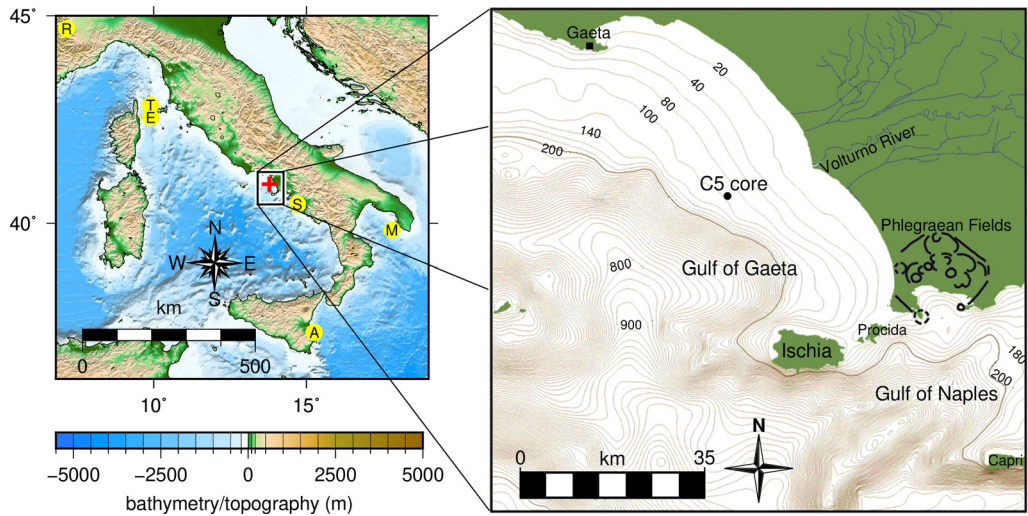


Fig. 1. (Left) The location of the C5 coring site. The box marks the study area on the Italian coast of the Tyrrhenian Sea. The red cross within the box marks the location of the C5 core. The yellow circles mark the previous palaeomagnetic core records from the region: A, cores MS06 and MS06-SW from Augusta Bay (Sagnotti *et al.* 2011), used as the main comparison curve in the present work; E, core ET91-18 (Vigliotti 2006); M, core MP49 (Béguin *et al.* 2019); R, cores RMD1 and RMD8 (Zanella *et al.* 2018); S, core C1201 from the Gulf of Salerno (Iorio *et al.* 2009); T, core ET95-4 (Vigliotti 2006). (Right) The location of the C5 core within the study area. Numerical labels on the bathymetry contours denote the water depth in metres.

Methods

Sampling and magnetic measurements

The 7.1 m C5 core was retrieved on 30 January 2013 from a water depth of 93 m using a Kullenberg gravity coring system during the AMICA2013 oceanographic cruise of the R/V *Urania-CNR*, part of the NextData project; the present study focuses on the uppermost 4.4 m of the core, since this is the interval for which age control is available. Onboard, the magnetic susceptibility was measured on split cores at 1 cm intervals using a Bartington MS2F point probe attached to an MS3 meter. Standard-sized u-channels were taken from the split cores, transported to the INGV palaeomagnetic laboratory in Rome and stored in a refrigerated container prior to measurement. At INGV, magnetic susceptibility was remeasured using a 47 mm Bartington MS2C loop sensor attached to an MS2 magnetic susceptibility meter, and stepwise alternating-field (AF) demagnetization of the natural remanent magnetization (NRM) was performed at steps of 5, 10, 15, 20, 25, 30, 40, 50, 60, 80 and 100 mT. The same AF demagnetization steps were used to demagnetize anhysteretic remanent magnetization (ARM), applied at an AF intensity of 100 mT and DC bias field of 50 µT. A 900 mT isothermal remanent magnetization (IRM) was then imparted, using the same AF steps to demagnetize the core for the third time.

Demagnetization studies were performed using a narrow-access pass-through cryogenic magnetometer (2G Enterprises model 755R) with an internal diameter of 42 mm, equipped with an inline AF demagnetizer and ARM unit, and housed in a Lode-star Magnetics shielded room. Cryomagnetometer measurements were taken at 1 cm intervals; however, the lengths of the sampling functions of the x-, y- and z-axis magnetometers were 4.09, 4.16 and 6.67 cm, respectively, so the effective resolution is somewhat lower.

The semi-liquid uppermost 20 cm of the core was excluded from the analysis, where coring disturbances had heavily distorted the sediments and, thus, the magnetic record. In addition, the uppermost and lowermost 4 cm of each u-channel were excluded from analysis, as the magnetometer's sampling function extends beyond the nominal sample position, making the end measurements unreliable; this procedure is standard in long core studies (see e.g. Blum 1997). The data were truncated at a depth of 440 cm, just below the level of the oldest dated layer. After these exclusions, 393 measurements remained for analysis.

Rock magnetic analysis of subsamples was conducted from the cores to inform our interpretation of the palaeomagnetic results. Using a Micromag 3900 vibrating sample magnetometer, hysteresis loops and IRM curves were measured on 27 samples taken at depths of 2, 22, 42, 51, 62, 82, 112, 162, 182,

202, 242, 262, 302, 317, 342, 367, 382, 417 and 422 cm, as well as one suite of first-order reversal curves (FORCs) (Pike *et al.* 1999; Roberts *et al.* 2014) from a sample taken at a depth of 10 cm. The IRM was imparted at 50 non-linearly spaced field strengths from 0 to 1 T, followed by backfield DC demagnetization at the same inverted field strengths, with an averaging time of 1 s. IRM results were used to calculate the remanent coercivity spectrum, coercivity of remanence (B_{cr}) and the remanent acquisition coercive force B'_{cr} for each sample. Hysteresis curves were measured from -1 to 1 T with a field increment of 10 mT and an averaging time of 300 ms. Median destructive field (MDF) values were also calculated from the AF demagnetization data.

The temperature dependence of magnetic susceptibility for samples taken at depths of 2, 62, 112, 162, 202, 242, 302 and 442 cm was investigated in order to further constrain the mineralogy. These experiments were performed on an Agico MFK-1A kappabridge with CS-3 furnace apparatus, and consisted of repeated susceptibility measurements taken at approximately 25 s intervals on samples heated in an argon atmosphere from room temperature to 700°C and cooled back to room temperature at a heating/cooling rate of approximately 10°C min $^{-1}$.

PSV and RPI records

Demagnetization data was analysed using the PuffinPlot application (Lurcock & Wilson 2012). The demagnetization data was visualized using Zijderveld (1967) diagrams, equal-area plots and demagnetization–magnetization plots. Principal component analysis (PCA) was used (Kirschvink 1980) to produce best-fit lines for the palaeomagnetic directions, and associated maximum angular deviation (MAD) values were calculated to assess the goodness of fit of the PCA directions. For the PCA calculations, an unanchored fit to the 15–60 mT demagnetization steps was used. For samples in the C5D core subsection (depths 352–451 cm), the 30 mT step was excluded from analysis due to a flux jump.

The absolute azimuthal orientation of the C5 core could not be measured during coring, nor was the relative azimuthal orientation (i.e. core section rotation) maintained between successive core sections. A recently-added feature (Lurcock & Florindo 2019) in PuffinPlot was used to reconstruct a declination record from the core sections: after fitting a PCA direction to each sample, the Fisherian mean directions for the topmost and bottommost 10 samples (hereafter referred to as the ‘top zone’ and ‘bottom zone’) were calculated for each core section. The declinations of each core section were rotated as a block in order to align the mean declination of its top zone with the mean direction of the bottom zone of the section above it. The declinations of

the core as a whole were then rotated so as to give a mean declination of zero.

Five estimates of RPI were produced, normalized to magnetic susceptibility, stepwise AF demagnetization of an ARM or stepwise AF demagnetization of an IRM. For each of the two stepwise normalizers, two alternative RPI estimates were calculated using different techniques. The first technique used the gradient method, whereby the RPI is determined from the slope of a linear regression between NRM demagnetization steps and their corresponding ARM steps (e.g. Channell *et al.* 2002; Xuan & Channell 2009); and the second technique used the mean of the ratios between the corresponding steps (e.g. Channell *et al.* 1997; Xuan & Channell 2009). For ARM-based estimates, the analysed steps were 5–60 mT inclusive; for IRM-based estimates, they were 15–100 mT inclusive. These limits were chosen by analysis of R^2 values associated with the linear regressions, and were selected to keep the minimum R^2 throughout the core as high as possible, with the additional constraints that the steps must be contiguous, the minimum step must be ≤ 20 mT and the maximum step must be ≥ 60 mT.

To assign ages to our palaeomagnetic data, an age model was constructed from age–depth tie-points (Table 1) that Margaritelli *et al.* (2016) established on the basis of biostratigraphy, tephra layers and isotope data. Three tie points were established at tephra layers in the core which were identified with known dated volcanic events on the basis of lithological and geochemical characteristics: the 1906 CE Vesuvius eruption at 52 cm bsf (cm below seafloor) (Mastrolorenzo *et al.* 1993; Barsotti *et al.* 2015); the Astroni3 event at 4297–4098 years BP (Smith *et al.* 2011); and a correlative of the Agnato Monte Spina Campi Flegrei eruption at 4420 ± 58 years BP (Lirer *et al.* 2013). Three biostratigraphic tie points were also determined: the abundance peak of *Globorotalia truncatulinoides* left uncoiled at 1718 ± 10 yr BP (Lirer *et al.* 2014), and the base and top of the acme interval of *Globigerinoides quadrilobatus* at 3700 ± 48 and 2700 ± 48 years BP, respectively (Lirer *et al.* 2013). Five further tie points were determined by correlation of the $\delta^{18}\text{O}_{G.ruber}$ record to the corresponding record from the C90 core retrieved in the Gulf of Salerno (Lirer *et al.* 2014). Linear interpolation was used to assign ages between the tie points.

Evaluation of data

As an initial check on the reliability of the demagnetization results, the mean inclination of our data was calculated and compared with mean inclination estimates for the same time period as predicted by the CALS10k.2 (Constable *et al.* 2016) and SHA.D-IF.14k (Pavón-Carrasco *et al.* 2014) models; the

Table 1. Tie points used to construct the C5 age model (columns 2 and 3), from Margaritelli et al. (2016)

Index No.	Depth (cm bsf)	Age (years BP)	Uncertainty (years)	Event	Reference	Tuned age (years BP)	Tuned offset (years)
1	52	44	0	Vesuvius tephra layer	Margaritelli et al. (2016)	44	0
2	87	232	10	Abundance peak <i>Globorotalia truncatulinoides</i>	Lirer et al. (2014)	233	-1
3	160	750	30	$\delta^{18}\text{O}$ correlation	Lirer et al. (2014)	760	-10
4	193	1049	38	$\delta^{18}\text{O}$ correlation	Lirer et al. (2014)	1042	7
5	226	1300	38	$\delta^{18}\text{O}$ correlation	Lirer et al. (2014)	1302	-2
6	254	1613	30	$\delta^{18}\text{O}$ correlation	Lirer et al. (2014)	1611	2
7	293	2371	29	$\delta^{18}\text{O}$ correlation	Lirer et al. (2014)	2349	22
8	322	2700	48	Top acme <i>Globigerinoides quadrilobatus</i>	Lirer et al. (2013)	2693	7
9	400	3700	48	Base acme <i>Globigerinoides quadrilobatus</i>	Lirer et al. (2013)	3691	9
10	414	4198	100	Astroni 3 tephra layer	Smith et al. (2011)	4200	-2
11	430	4420	58	Agnano Monte Spina tephra layer	Lirer et al. (2013)	4424	-4

The index numbers correspond to those shown in Figures 7 and 8. The final two columns refer to the tuning procedure used to compare our data with previous regional records; details are given in the subsections ‘Evaluation of data’ (in the Methods section) and ‘Results of curve matching’ (in the Results section). The term ‘ $\delta^{18}\text{O}$ correlation’ in the fifth column denotes graphic correlation of $\delta^{18}\text{O}_{G.\text{ruber}}$ with the isotope record of the C90 core (Lirer et al. 2013, 2014). Note that the depths in this table are offset by 6 cm relative to those in Margaritelli et al. (2016), which uses a composite depth scale rather than (as in the present work) the depth within the C5 core. Ages in this table correspond to the BC/BCE dates given in column 3 of table 5 in Margaritelli et al. (2016). Some ages in this table differ from the corresponding ages in column 4 of table 5 in Margaritelli et al. (2016) due to typographical errors in the latter, as does the uncertainty of tie point 6.

common procedure of checking the inclination against that predicted by a geocentric axial dipole model is less appropriate in this case, since the time span may be insufficient to fully average out the secular variation. Mean inclinations were calculated using the Arason–Levi maximum-likelihood method (Arason & Levi 2010) to avoid the shallowing bias which can be introduced when taking the arithmetic mean of the inclination values.

In order to further explore the compatibility of the C5 magnetic records with previously published data, a curve-matching technique was applied. Curve-matching techniques are more commonly applied for dating, using a reliably dated reference curve as a target (e.g. Vigliotti et al. 2008), and are often used (under the name ‘tuning’) to fit data to an astronomical age model. In our case, we already have a reasonably precise age model, and the variation between the available comparison curves, and between them and our record, suggested that curve matching would be of limited value in improving the age model. Using

the magnetic data themselves to improve their own age model would also mean that the records would no longer be fully independent. However, curve matching still has value in evaluating to what extent our records can be reconciled with previously published data within the constraints imposed by our age–depth control points. Effectively, the process produces a hypothetical improved age model in which the reconstructed sedimentation rate is allowed to vary between the control points in order to produce a better match to a reference curve. Our use of the term ‘reference curve’ here merely denotes that the curve, during the matching procedure, is held constant, and does not indicate an automatic assumption that this reference curve is necessarily more accurate than our own data; the tuning procedure is here used purely for intercomparison, not for improvement on the basis of a known better record. When considering a discrepancy between our data and another record, a curve-matched age model can help to distinguish between a genuine difference in palaeofield

behaviour and a misalignment caused by the limited resolution of our linear age model.

In this experiment, the Augusta Bay curves of Sagnotti *et al.* (2011) were the obvious choice for the reference data: high-resolution, relatively nearby records which showed reasonable agreement with the C5 data under the linear age model. The temporal extent of the C5 records extends slightly beyond that of the Augusta Bay records (4174–150 years BP), so composite reference curves were created by extending the relocated Augusta Bay records with data generated from the CALS10k.2 model for the periods 4570–4150 and 155–0 years BP. In the intervals 4150–4050 and 250–155 years BP, linear smooth transitions were imposed between CALS10k.2 data and the Augusta Bay records.

Curve matching was performed using the Match software of Lisiecki & Lisiecki (2002), allowing us to produce an objectively determined, reproducible age model which optimized the correlation simultaneously for the declination, inclination and intensity records. The Match program divides each time series to be analysed into a large number of intervals and uses a dynamic programming technique to determine a sequence of sedimentation rates which will produce a globally optimal match with a corresponding reference curve. The algorithm providing a quantitative assessment of the goodness of a candidate match is parametrized by a collection of user-configurable settings. For our analysis, the same parameters were used for each of the declination, inclination and RPI series: relative sedimentation rates of 1:9, 1:8, 1:7, 1:6, 1:5, 1:4, 1:3, 2:5, 1:2, 3:5, 2:3, 3:4, 4:5, 1:1, 5:4, 4:3, 3:2, 5:3, 2:1, 5:2, 3:1, 4:1, 5:1, 6:1, 7:1, 8:1 and 9:1, 200 intervals, a no-match penalty of 10, a speed penalty of 0, a relative target speed of 1:1, a speed change penalty of 5.5, a tie penalty of 0.065 and a gap penalty of 1, with even weighting between all three datasets. This automated approach can be contrasted with the traditional, and still frequently used, technique of correlating visually identified features (e.g. minima and maxima) in PSV or RPI curves. Visual correlation becomes difficult to perform when (as in the present study) multiple parameters must be matched simultaneously. It also introduces an inevitable subjective element, making reproducibility difficult or impossible. In addition, our reference curve for this study was relatively local and of high resolution; in such cases, automated curve matching can make fuller use of the available data, rather than concentrating on a small set of predefined features.

We used the tie points listed in Table 1 as constraints for the curve-matched age model. Each tie-point age has an associated uncertainty. We were able to accommodate this uncertainty in the Match software by means of the ‘tie penalty’ parameter, which controls the amount by which the specified

tie points are allowed to move. This parameter can only be adjusted globally, not per tie point; we therefore set it to the lowest possible value that kept all of the age-adjusted tie points within their uncertainty ranges.

Results

Rock magnetism

Ranges for the B_{cr} and B'_{cr} parameters calculated from the IRM results were, respectively, 28–40 and 37–50 mT, both well within the reference ranges for magnetite given by Peters & Dekkers (2003). In order to investigate the possibility of mixtures of magnetic phases within the samples, we analysed the IRM acquisition curves of 23 samples by fitting them to sums of cumulative log-Gaussian curves (Robertson & France 1994) using version 2.2 of the Irmunmix program (Heslop *et al.* 2002). In every case, a good fit was produced by a single log-Gaussian component with a peak at around 1.6–1.7 (corresponding to c. 40–50 mT), in agreement with the values given by Robertson & France (1994) for magnetite, suggesting that the remanence is carried by a single population of magnetite grains. Typical log-Gaussian fits for six of the analysed samples are shown in Figure 2. There was little variation in the magnetization gradient curves and fitted Gaussians between the studied samples, indicative of a consistent magnetic mineralogy throughout the core.

We analysed and plotted the FORC data using the FORCinel program (Harrison & Feinberg 2008). The results are shown in Figure 3. The horizontal spindle shape near the centre of the plot is consistent with an assemblage of non-interacting single-domain or pseudo-single-domain grains with differing coercivities spanning a continuous range (Roberts *et al.* 2000), suggesting that the analysed sample is suitable for palaeomagnetic study.

Coercivity and magnetization parameters show very little variation throughout the core, with the great majority of the samples having $2.3 < B_{cr}/B_c < 2.6$ (where B_c is the coercive force) and $0.18 < M_{rs}/M_s < 0.21$ (where M_{rs} is the saturation remanent magnetization and M_s is the saturation magnetization); this supports the inference from the IRM unmixing results that the magnetic mineralogy is consistent. Low-field magnetic susceptibility was consistent throughout most of the core, with the exception of four susceptibility spikes at around 53, 236, 380 and 439 cm bsf. The spikes at 53, 380 and 439 cm bsf are associated with identified tephras; the spike at 236 cm bsf does not correspond to a known tephra but occurs directly above a distinct dark layer in the core, suggesting that it is associated with a mineralogical change. Lithological and susceptibility logs for the core are shown in Figure 4.

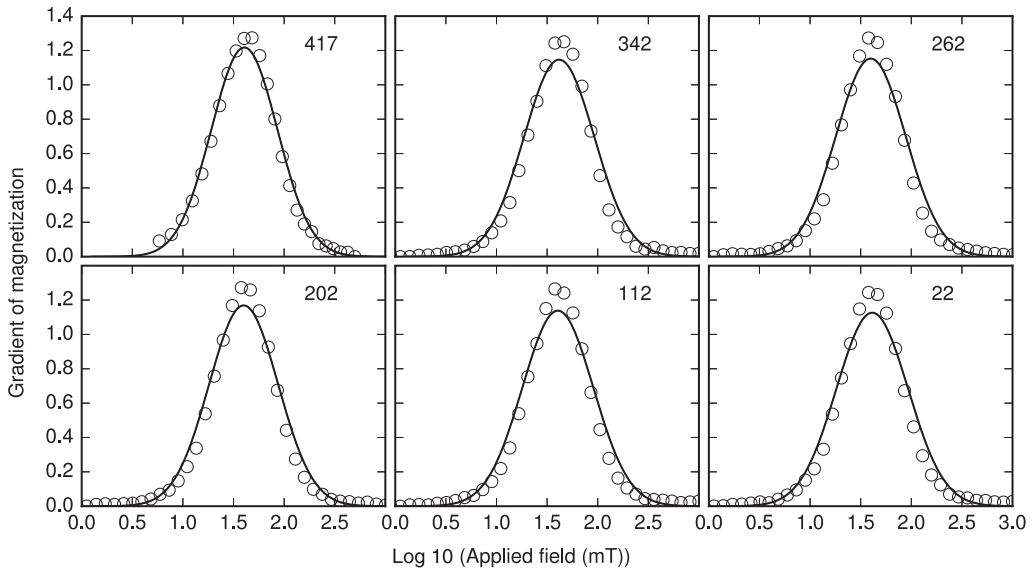


Fig. 2. Typical single-component cumulative log-Gaussian fits to IRM acquisition data from six of the 23 samples subjected to IRM analysis. Points are gradients of the measured IRM acquisition curve; lines are the best-fit Gaussian curves. Numbers in the top right of subplots indicate the sample depth in cm bsf.

Temperature dependence of magnetic susceptibility results were similar across all eight samples subjected to kappabridge analysis (Fig. 5): susceptibility rose slightly during heating with a broad peak in the 400–500°C range, dropped to a minimum at slightly under 600°C and underwent no further change during heating or cooling in the 600–700°C range. On cooling, susceptibilities began to rise at temperatures below 600°C and followed similar paths to the heating curves, but with susceptibilities approximately 2–3 times greater. Curie points were determined using a linear fit to inverse susceptibility, as described by Petrovský & Kapička (2006), and all lay in the range 561–584°C. The differing heating and cooling curves indicate that heating-induced alteration took place during analysis despite the use of an argon atmosphere, making exact mineral identification more difficult. The results, in particular the Curie temperatures, are nevertheless consistent with magnetite being the main remanence carrier, possibly with minor cation substitution lowering the Curie temperature. The similarity of the heating and cooling curves across all the thermally analysed samples provides further confirmation of a consistent magnetic mineralogy throughout the studied core sections.

Demagnetization behaviour and palaeomagnetic secular variation

Figure 6 shows Zijderveld, equal-area and demagnetization-intensity plots of some typical

demagnetization paths for selected samples, and Figure 7 marks the positions of those samples on depth-inclination and depth-declination plots. Demagnetization characteristics showed suitability for reliable determination of a palaeomagnetic direction, with almost all samples having a single, strong magnetic component trending directly towards the origin during stepwise demagnetization. Calculated MDF values were all in the range 19–34 mT, with a mean of 24 mT; within the range of values for magnetite MDFs reported by Heider *et al.* (1992). The demagnetization behaviour is thus consistent with the results of the rock magnetic experiments, which indicated a single population of PSD magnetite as the dominant remanence carrier.

The MAD values that were calculated in this study to assess the goodness of fit confirmed the quality of the data: the mean MAD value was 1°, all but 21 samples had a MAD below 2° and the maximum MAD was 4.98°. MAD values <10° are generally considered ‘reasonably good’ (McElhinny & McFadden 2000, section 3.4.3) and <5° ‘highly reliable’ (e.g. Johnson *et al.* 1998). MAD values are shown along with declinations and inclinations in Figure 7. Because of the linear, origin-directed demagnetization paths, varying the points selected for PCA or the anchoring parameter caused only minimal variation in the calculated directions, giving further confidence in the reliability of the directional estimates.

As described in the earlier subsection ‘Evaluation of data’, the inclinations of the core data were

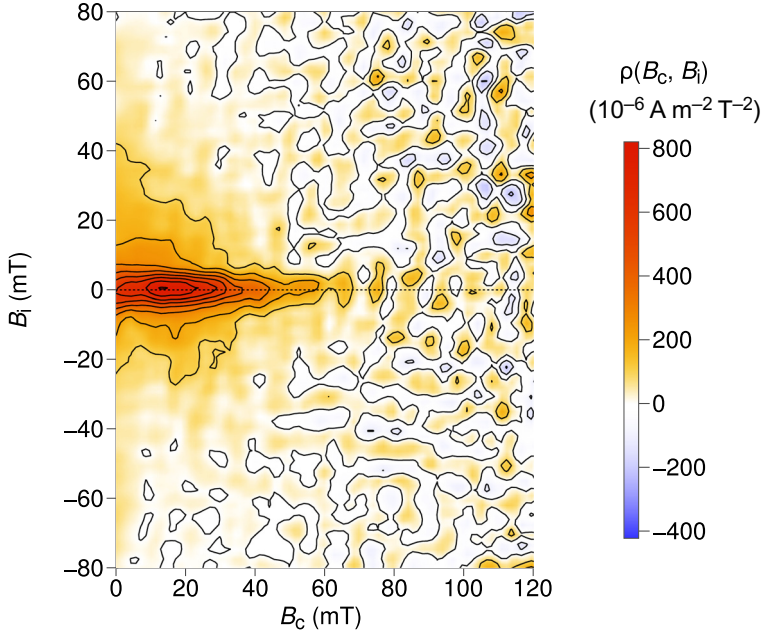


Fig. 3. Results of FORC analysis on a sample from the uppermost part of the C5 core, produced using version 2.0 of the FORCinel program (Harrison & Feinberg 2008) running under version 6.3.7.2 of the Igor Pro environment. A smoothing factor of 5 was used. Saturation magnetization was estimated by paramagnetic slope correction. Data were corrected for drift and for first-point artefact. B_i , interaction field; B_c , coercivity; ρ , FORC density.

compared with results from the CALS10k.2 and SHA.DIF.14k models. The mean inclination of the C5 data is 57.1° ; both models give a mean inclination of 59.7° , showing that the inclination data are consistent with the modelled field for this site. The slight discrepancy may be attributable to inclination-shallowing processes (e.g. Brennan 1993).

Figure 7 shows a comparison between the C5 PSV directions (plotted on a depth scale) and selected regional core and model data (plotted on an age scale), along with the tie points used for the age model, MAD values, core boundaries and depths of the samples whose demagnetization data are shown in Figure 6. Model data were generated directly for the C5 coring site, and sedimentary PSV records were relocated to the site using the ‘conversion via pole’ (CVP) method (Noel & Batt 1990). An additional correction was applied to the Augusta Bay record, which is strongly affected by inclination shallowing, estimated at $10\text{--}20^\circ$ by Sagnotti *et al.* (2011): we corrected for this shallowing by adding a fixed offset of 8.23° , calculated by subtracting the mean of the measured inclinations from the mean inclination for the same time period as calculated by the CALS10k.2 model. The comparison curves are covered in more detail in the Discussion.

The PSV inclination record is marked by a sequence of very large, abrupt swings in the 230–250 cm bsf interval. This feature coincides with a dark layer and large susceptibility spike in the core (Fig. 4), and with spikes in ARM-based RPI reconstructions (see below). These observations all point to a mineralogical change in the core (possibly the presence of greigite), rendering the palaeomagnetic results unreliable within this zone. The abrupt changes in inclination may in this case be due to the behaviour of the magnetometer response function in the presence of large magnetization changes (e.g. Guyodo *et al.* 2002). For this reason, we excluded data from the 230–250 cm bsf interval from further consideration.

Relative palaeointensity

Figure 8 shows our RPI estimates from C5 core data plotted against depth, alongside several published regional RPI estimates and model results plotted against time; the comparison curves are covered in more detail in the Discussion. The RPI curves comprise two ARM-normalized RPI estimates, two IRM-normalized estimates and one estimate normalized to magnetic susceptibility (as described in the

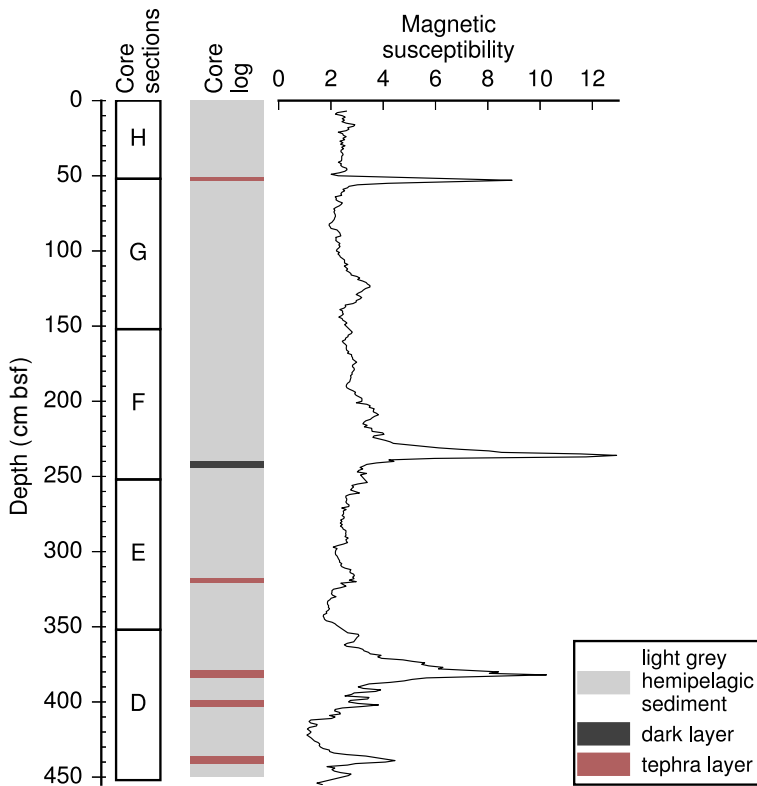


Fig. 4. Lithological and magnetic susceptibility logs for the C5 core. Magnetic susceptibility is in arbitrary units.

Methods). The mean of the R^2 values associated with the gradient-based ARM-normalized estimates is 0.996, and the corresponding mean of R^2 values for the IRM-normalized estimates is 0.959, indicating generally high-quality fits for both sets of estimates. The five estimates are mostly in reasonably good agreement, with the exception of a small number of obvious outliers in individual records. Both IRM-normalized records diverge from the others at two points, at around 156 and 176 cm; the mean ratio-based IRM-normalized record additionally diverges at 363 cm. We attribute these discrepancies to the fact that the IRM was measured at a later date than the rest of the core data, creating the possibility of contamination, diagenesis or oxidation of core material while in storage. The fact that two of the discrepancies are very near core-section ends is consistent with this hypothesis. The ARM-based estimates diverge from the consensus at only one point, around 236 cm; like the corresponding inclination variations, this is probably an artefact of a mineralogical change associated with the dark layer in the core. The RPI estimates fulfil several criteria for reliability, as outlined by Tauxe (1993): strong evidence of magnetite as the remanence carrier, minimal

inclination error, a single remanence component, straightforward demagnetization characteristics and only moderate variation in concentration (even at the tephra peaks, the susceptibility remains well within an order of magnitude of the usual values), agreement between different normalization methods (excepting the few outliers mentioned above), and (as mentioned in the Discussion) agreement with other records from the region.

Dated palaeomagnetic results

We dated our palaeomagnetic results using a linear age model as described in the Methods. The palaeomagnetic data are plotted against age in Figure 9, along with the core and model data from Figures 7 and 8 for comparison. We explore the relationship between our data and the previously published records in the discussion. The RPI record shown in Figure 9 is synthesized from the five normalized estimates by taking the median normalized value at each depth. This technique produces a consensus record excluding the occasional, probably spurious, peaks that only appear in one or two of the estimates, as

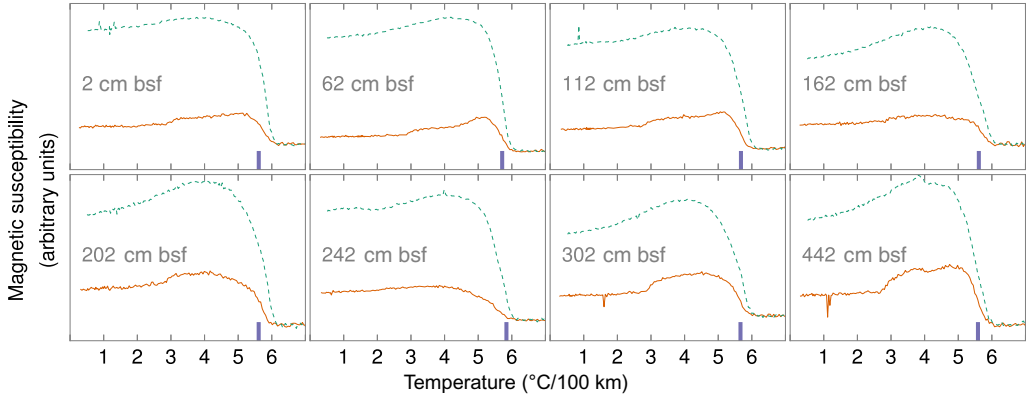


Fig. 5. Results from experiments on the temperature dependence of magnetic susceptibility. Measured susceptibilities have been corrected for the susceptibility of the empty furnace. Sample depths are superimposed on plot backgrounds. Solid orange lines are heating curves; dashed green lines are cooling curves. Purple bars at the bottom of plots indicate estimated Curie temperatures obtained by linear fit to inverse susceptibility.

described in the ‘Relative palaeointensity’ subsection of the Results.

Results of curve matching

We compared our results with a composite Augusta Bay/CALS10k.2 record using a curve-matching procedure as described in the ‘Evaluation of data’ subsection of the Methods. The results are shown in Figure 10, along with a reconstruction of the sedimentation rate implied by the curve-matched age model. Table 1 lists the original and adjusted tie points, along with their associated uncertainties and adjustment offsets.

Discussion

Overview of records suitable for comparison with C5 results

The most suitable published record for comparison with the C5 core comes from the Augusta Bay cores MS06 and MS06-SW analysed by Sagnotti *et al.* (2011). These cores provide a near-continuous, 4 kyr record from eastern Sicily in the Ionian Sea. We use these data as the main point of comparison for our own results, since they have a high resolution, cover almost the entire time span of the C5 core, include both PSV and RPI records, and were obtained from a location less than 450 km away from the C5 coring site.

Also of relevance are the PSV records of two cores from the northern Tyrrhenian Sea, ET91-18 and ET95-4 (Vigliotti 2006), and the PSV and RPI records of core C1201 from the Gulf of Salerno

(Iorio *et al.* 2009). We included these in the comparisons as they were retrieved relatively close to the C5 coring location (under 400 km in the case of the northern Tyrrhenian cores, and under 100 km for core C1201) and cover most of the time span represented by the C5 core. Unfortunately, their temporal resolution is too low to allow detailed comparison with our results but they are, nevertheless, useful for intercomparison of longer-term trends. For further comparison, we also include the MP49 core record from the Gulf of Taranto (Béguin *et al.* 2019), the RMD1 and RMD8 speleothem records from northern Italy (Zanella *et al.* 2018), and a compendium of Italian archaeomagnetic and volcanic data downloaded from the GEOMAGIA50.v3.3 database on 31 March 2020 (Brown *et al.* 2015).

The locations of core records used for comparison are shown on the overview map in Figure 1, and the data are included in Figure 9. The data for the ET91-18 and ET95-4 cores were obtained from the supporting data of Nilsson *et al.* (2014).

Several well-established regional reference curves (‘master curves’) exist for PSV dating in Europe, based both on archaeological artefacts and sedimentary records; in western Europe, the 10 kyr UK master curve (Turner & Thompson 1981) and the western European 3 kyr archaeomagnetic curve (Bucur 1994; Daly & Le Goff 1996; Gallet *et al.* 2002) are among the most widely used. To date, there is no corresponding master curve for the Italian region, although efforts are under way to construct one (Tema *et al.* 2006; Vigliotti 2006). We therefore include the western European curve in our comparison as the most suitably located regional master curve.

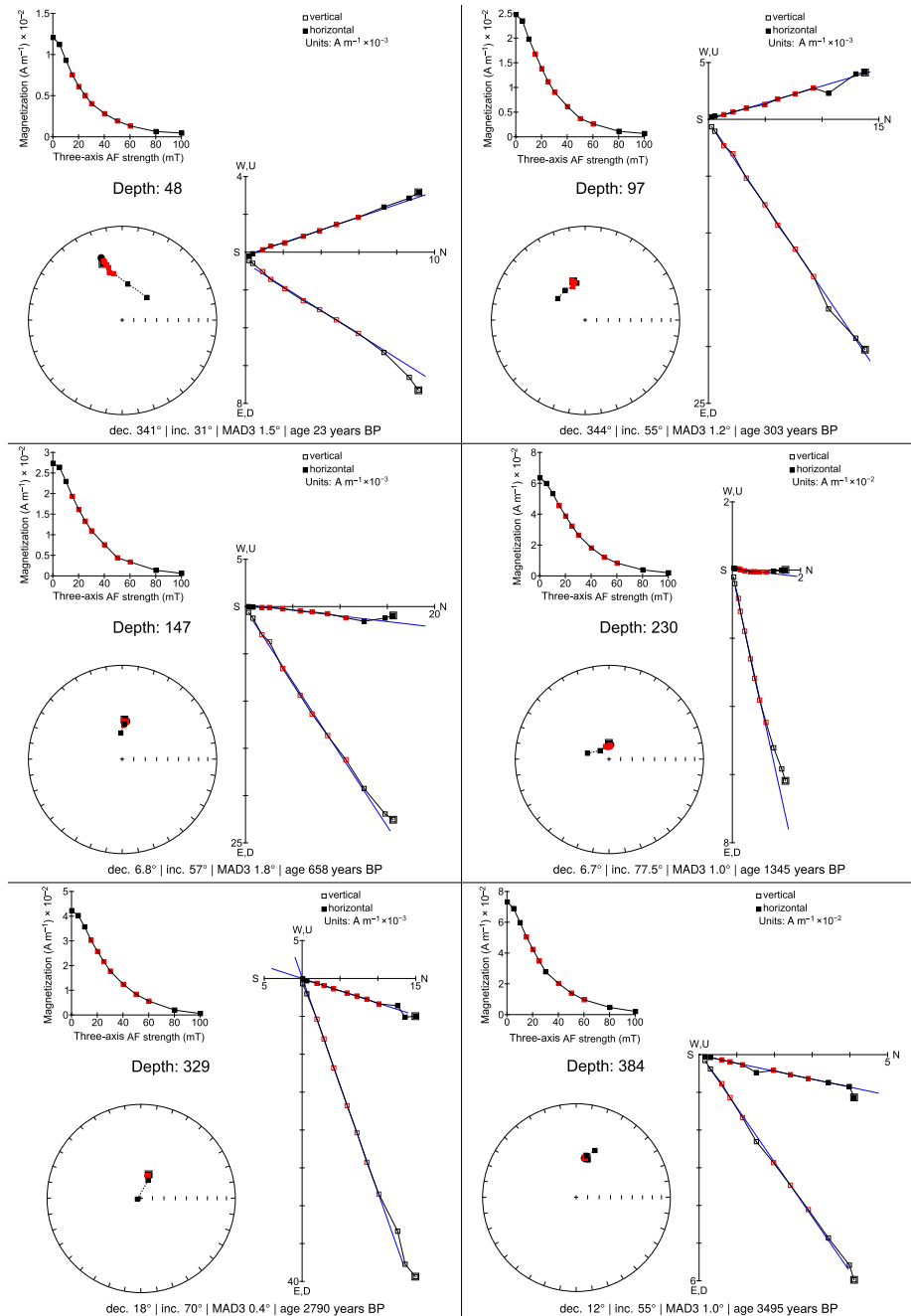


Fig. 6. Typical sample behaviour during stepwise alternating-field demagnetization of the natural remanent magnetization at various depths throughout the core. Intensity plots show a decrease in magnetization with progressive treatment steps; equal-area plots show the direction of magnetization vectors; Zijderveld plots show the orthogonal projections of three-dimensional demagnetization vectors. Depths are given in cm bsf, and are highlighted on the inclination curve in Figure 7. Solid points are projections onto the horizontal plane; open points are projections onto the vertical north–south plane; note that this projection slightly steepens the apparent inclinations of the demagnetization lines. Blue lines are projections of the best-fit vector as determined by principal component analysis (PCA). Red data points indicate demagnetization steps which were selected for PCA.

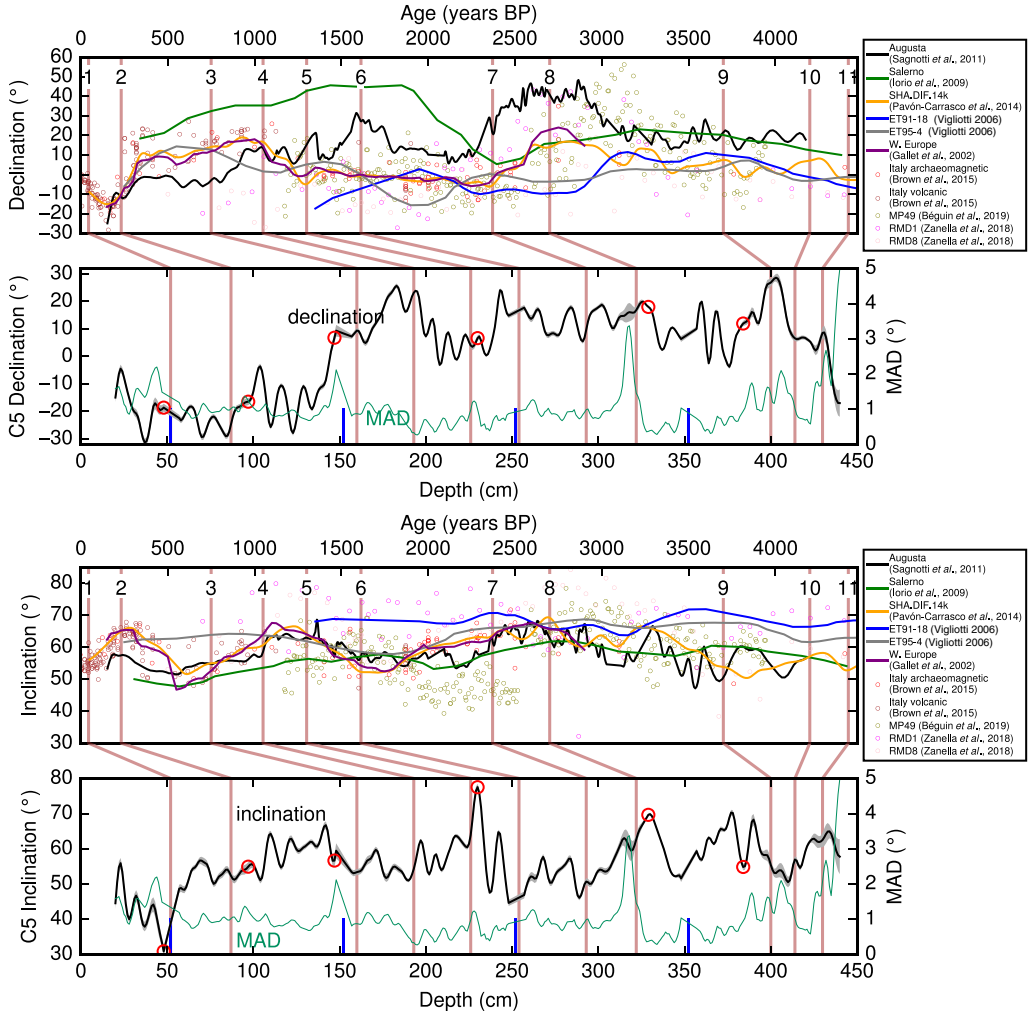


Fig. 7. Comparison between C5 PSV directions and selected reference curves and models. The upper pair of plots shows declination and the lower pair shows inclination. In each plot pair, the upper plot shows reference data against age, and the lower plot shows C5 core data against depth. Comparison curves are as follows: Augusta, Sicilian Augusta Bay core record (Sagnotti *et al.* 2011); Salerno, C1201 core from Salerno Bay (Iorio *et al.* 2009); SHA.DIF.14k, PSV model by Pavón-Carrasco *et al.* (2014); ET91-18, northern Tyrrhenian ET91-18 core record (Vigliotti 2006); ET95-4, northern Tyrrhenian ET95-4 core record (Vigliotti 2006); W. Europe, western European archaeomagnetic curve (Gallet *et al.* 2002); Italy archaeomagnetic, Italian archaeomagnetic data from GEOMAGIA50.v3 (Brown *et al.* 2015); Italian volcanic, Italian volcanic data from GEOMAGIA50.v3 (Brown *et al.* 2015); MP49, MP49 core from Taranto Gulf (Béguin *et al.* 2019); RMD1, Rio Martino Cave core RMD1 (Zanella *et al.* 2018); RMD8, Rio Martino Cave core RMD8 (Zanella *et al.* 2018). Directions from core records relocated to the C5 site. Model results generated for the C5 location. Red-brown vertical lines indicate age control points from Margaritelli *et al.* (2016), and are labelled with numbers corresponding to those in Table 1. The depth plots also show MAD values indicating the quality of the demagnetization data, both as a separate green line on an expanded vertical scale, and as a grey area surrounding the inclination and declination curves (the grey area is mostly invisible due to its small extent). Extended blue ticks at the bottom of the depth plots indicate core section boundaries. Red circles indicate depths for which demagnetization results are shown in Figure 6.

When comparing palaeomagnetic records from different locations, it is important to consider the potential errors introduced by relocation of the

data. The CVP method partially compensates for the latitudinal dependence of the dipole component of the geomagnetic field but does not take higher-order

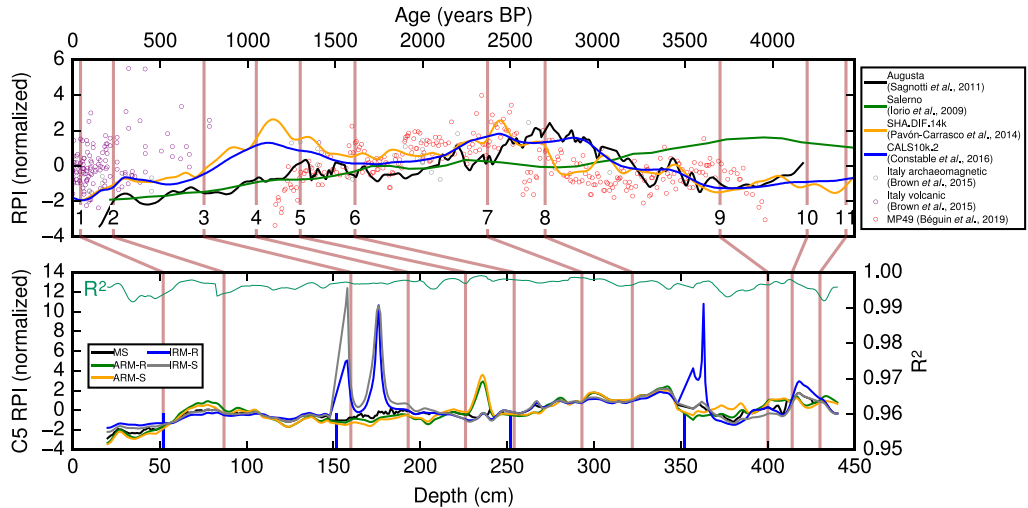


Fig. 8. Comparison between C5 RPI estimates (lower plot) and selected reference curves and models (upper plot). Comparison curves are as follows: Augusta, Sicilian Augusta Bay core record (Sagnotti *et al.* 2011); Salerno, C1201 core from Salerno Bay (Iorio *et al.* 2009); SHA.DIF.14k, SHA.DIF.14k model results (Pavón-Carrasco *et al.* 2014); CALS10k.2, CALS10k.2 model results (Constable *et al.* 2016); Italy archaeomagnetic, Italian archaeomagnetic data from GEOMAGIA50.v3 (Brown *et al.* 2015); Italy volcanic, Italian volcanic data from GEOMAGIA50.v3 (Brown *et al.* 2015); MP49, MP49 core from Taranto Gulf (Béguin *et al.* 2019). The lower plot shows the RPI of the C5 core estimated by five different methods: MS, normalization to magnetic susceptibility; ARM-R, normalization to ARM intensity using the mean of the NRM/ARM ratios at different demagnetization steps; ARM-S, normalization to ARM intensity using the slope of linear regression between the NRM and ARM demagnetization data; IRM-R, normalization to IRM intensity using the mean of the NRM/IRM ratios at different demagnetization steps; IRM-S, normalization to IRM intensity using the slope of linear regression between the NRM and IRM demagnetization data; also shown are the R^2 values associated with the linear regressions on the NRM and ARM data, as an indicator of data quality. Red-brown vertical lines represent age control points from Margaritelli *et al.* (2016), and are labelled with numbers corresponding to those in Table 1. Extended blue ticks at the bottom of the depth plot indicate core section boundaries.

field components into account. Casas & Incoronato (2007) investigated the potential errors introduced by CVP-based relocation. Their results indicate that, for the time period and geographical region relevant to the present study, relocation errors do not exceed 0.25° per 100 km. This implies maximum relocation errors of the order of 1° or less for the other Tyrrhenian core records which we compare with ours. Relocation of the western European curve from Paris to the C5 coring site involves a potential maximum error of around 3° , somewhat less than the 5° maximum error which Casas & Incoronato (2007) estimated for the error involved in the initial construction of the curve and relocation of data to Paris. While this is greater than the maximum relocation error among the Tyrrhenian cores, previous work has shown that, in practice, the western European curve corresponds reasonably well to Italian PSV (e.g. Arrighi *et al.* 2004; Speranza *et al.* 2006; Vigliotti 2006; Vigliotti *et al.* 2008).

Geomagnetic models can also provide useful comparisons with palaeomagnetic records, particularly where no suitable local reference curve is

available. Several new and updated models have been published in recent years; among the most relevant for the location and time span of the C5 core are SHA.DIF.14k (Pavón-Carrasco *et al.* 2014) and CALS10k.2 (Constable *et al.* 2016). Model results are necessarily limited in temporal and spatial resolution on the timescales involved in the analysis of the C5 core but their ability to generate data for a particular location over an extended time span can provide a useful check on more direct records. SHA.DIF.14k model results for the C5 location and time span are included in Figure 9; additionally, CALS10k.2 results are shown in the RPI plot as there are few RPI core records available for comparison.

Comparison of C5 results with previously published records

As can be seen from a comparison of the curves shown in Figure 9, the C5 PSV and RPI records are plausible with respect to comparable data for the region. Correlation between the RPI record and

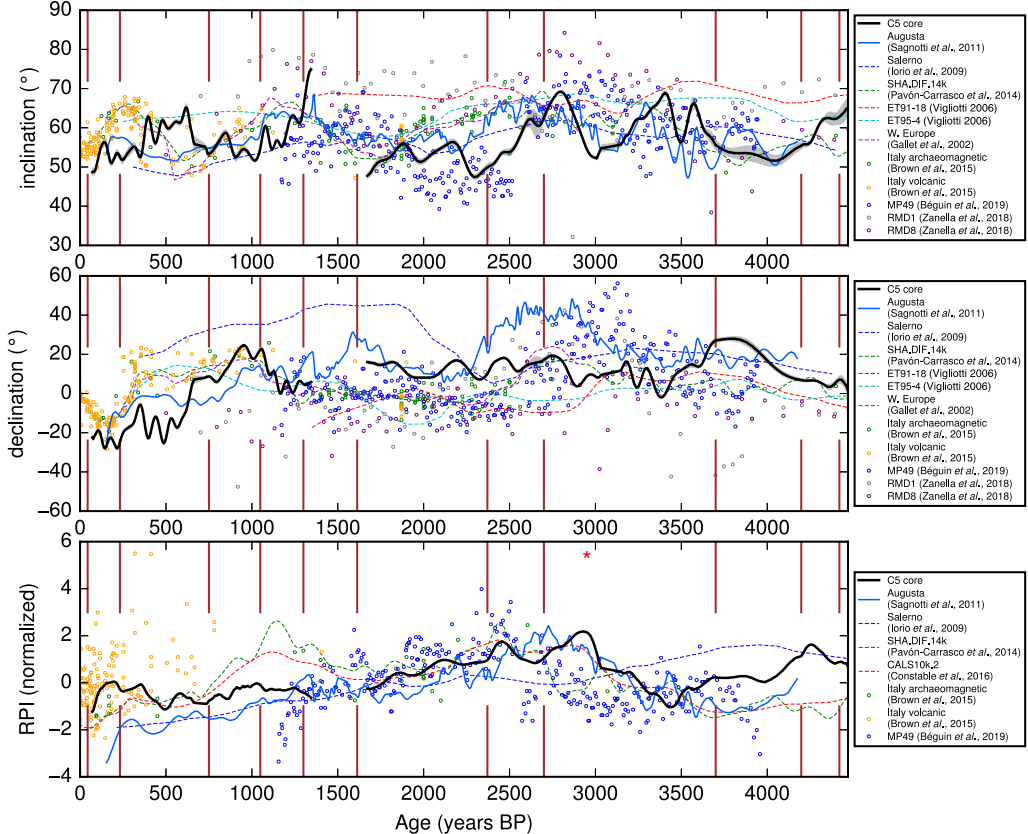


Fig. 9. PSV and RPI curves, dated by a piecewise linear age model constructed from the age control points shown in Table 1. PSV and RPI measurements from the C5 core are shown in black. The solid blue curve shows the Augusta Bay record of Sagnotti *et al.* (2011). Thin dotted lines and open circles show previously published records and model results for further comparison. Comparison curves are as follows: Salerno, C1201 core from Salerno Bay (Iorio *et al.* 2009); SHA.DIF.14k, SHA.DIF.14k model results (Pavón-Carrasco *et al.* 2014); ET91-18, northern Tyrrhenian ET95-4 core record (Vigliotti 2006); W. Europe, western European archaeomagnetic curve (Gallet *et al.* 2002); CALS10k.2, CALS10k.2 model results (Constable *et al.* 2016); Italy archaeomagnetic, Italian archaeomagnetic data from GEOMAGIA50.v3 (Brown *et al.* 2015); Italy volcanic, Italian volcanic data from GEOMAGIA50.v3 (Brown *et al.* 2015); MP49, MP49 core from Taranto Gulf (Béguin *et al.* 2019); RMD1, Rio Martino Cave core RMD1 (Zanella *et al.* 2018); RMD8, Rio Martino Cave core RMD8 (Zanella *et al.* 2018). Interrupted red-brown vertical lines indicate tephra and biostratigraphic age control points (Margaritelli *et al.* 2016) used to construct the age model. MAD values are shown as a grey area surrounding the inclination and declination curves (the grey area is mostly invisible due to its small extent). The red asterisk at c. 2950 years BP in the bottom plot marks an RPI peak coincident with the Levantine spike (see the Discussion). Data around 1500 years BP are not shown due to spurious artefacts (see the Results). Ages are relative to 1950.

the Augusta Bay curve is good throughout, and the declination and inclination records, while exhibiting some clear divergences at points, are also in broad agreement with the Augusta Bay data. Mean differences between C5 and Augusta bay declination, inclination and RPI are 11.5° , 5.1° , and 0.88, respectively. In evaluating the correlations, it should be kept in mind that, as can be seen from the additional curves in the plots, there is also considerable

divergence between previous geomagnetic records and model results for the Tyrrhenian Sea region.

The C5 RPI record mostly parallels the Augusta Bay curve, and where it diverges it still remains, throughout the great majority of the record, within the envelope of the other plotted curves. While there is a broad-scale agreement between the plotted curves, there is no close match and each curve diverges from the consensus in places. In the case

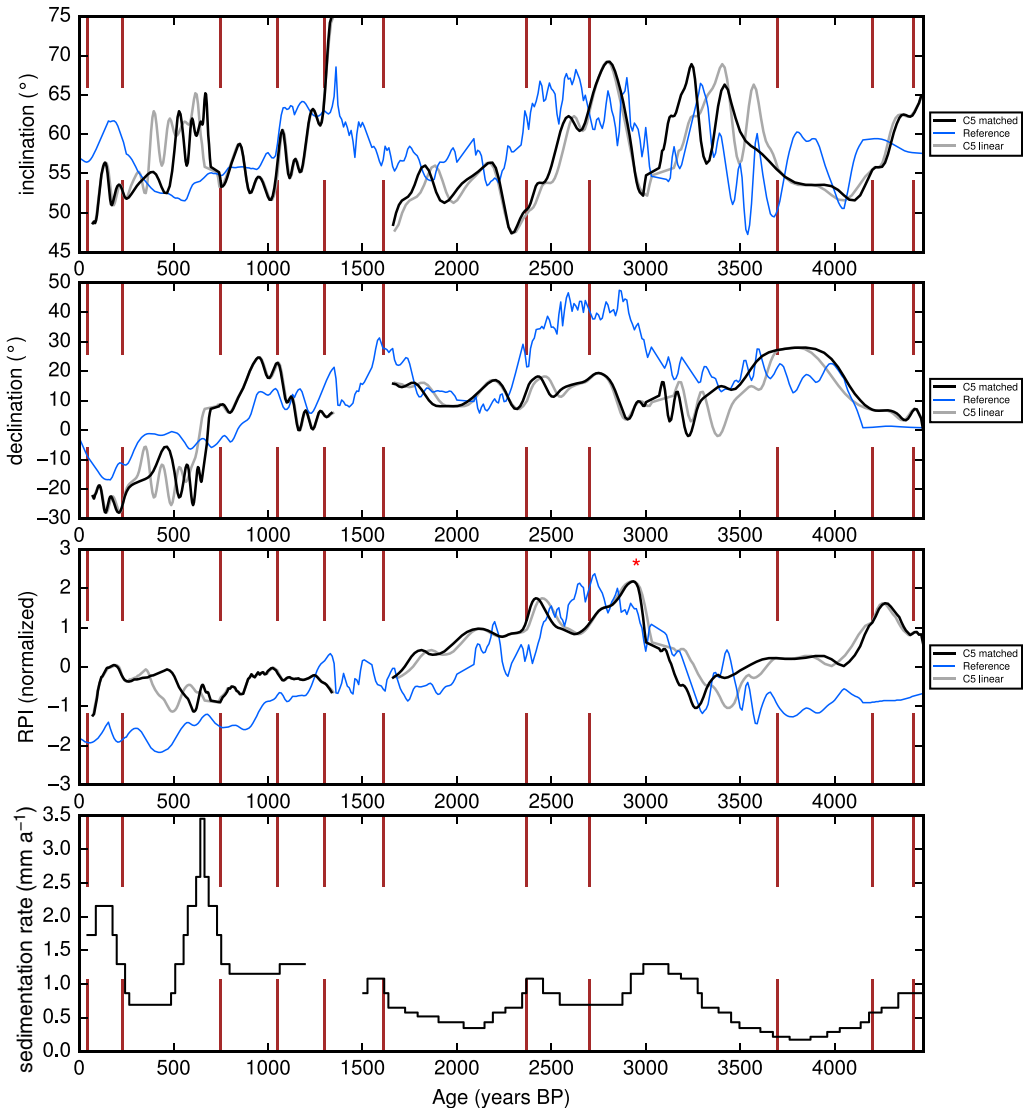


Fig. 10. Results of automated curve matching between measured declination, inclination and RPI, and corresponding reference curves, constrained by known age control points. Results of curve matching are shown in black and labelled ‘C5 matched’. Curves with linear age model (as used in Fig. 9) are shown in grey and labelled ‘C5 linear’. Curve matching was performed by tuning measurements from the C5 core to the reference curves shown in blue and labelled ‘Reference’, which are a composite of the data of Sagnotti *et al.* (2011) and the CALS10k.2 model (Constable *et al.* 2016) (see the subsection ‘Evaluation of data’ in the Methods). Interrupted red-brown vertical lines indicate tephra and biostratigraphic age control points (listed in Table 1) used to constrain the tuning. The red asterisk at c. 2950 years BP in the bottom plot marks an RPI peak coincident with the Levantine spike (see the Discussion). Data around 1500 years BP are not shown due to spurious artefacts (see the Results). Ages are relative to 1950.

of the C5 curve, the RPI is elevated compared to most of the comparison curves in the youngest 500 years BP but the behaviour does parallel a contemporary lower-intensity feature in the Augusta

Bay curve, and appears consistent with the collated Italian archaeomagnetic and volcanic data. Throughout most of the 3.8–1.3 ka BP interval, there is good agreement between the C5 curve, the MP49 core of

Béguin *et al.* (2019) and the GEOMAGIA Italian archaeomagnetic data, with all of them showing slow, parallel declines in intensity throughout the interval from 2.5 to 1.3 ka BP. There is similar agreement in the 3.8–3.2 ka BP interval. From 3.2 to 2.5 ka BP, the story is more complex: the C5, Augusta Bay and CALS10k.2 curves all show a similar increase in intensity, while the MP49 core dips strongly in the same interval. Here, and also at c. 3.9 and 1.2 ka BP, the MP49 curve is an marked outlier compared to the rest of the ensemble, suggesting that it may not represent an accurate record in these intervals. The large peak at c. 4.2 ka BP in the C5 curve is not mirrored in the lower-resolution comparison curves but the younger part of it correlates with an equally steep rise in the Augusta Bay record; since the Augusta Bay record does not extend beyond 4.174 ka BP, the older part of the peak cannot be compared with it. This portion of the record should, however, be treated with caution due to the presence of the Astroni 3 and Agnano Monte Spina tephra layers in this zone.

The RPI peak at c. 2.95 ka BP (1000 BCE) (marked with an asterisk in Fig. 9) is of particular interest. It is present in all five RPI estimates from all three normalizers, giving confidence that it represents a genuine RPI feature rather than an analysis artefact. Its age corresponds closely to that of the Levantine spike (Shaar *et al.* 2016, 2018; Korte & Constable 2018), a recently discovered and still incompletely understood feature found in some palaeointensity records. The Levantine spike was first identified from archaeomagnetic studies in Jordan (Ben-Yosef *et al.* 2009) and Israel (Shaar *et al.* 2011) as a transient decadal-scale event during which the geomagnetic field strength approximately doubled. Since then, potential correlative features have been found as far afield as China and Texas (Davies & Constable 2017 and references therein). It is possible that the contemporaneous rapid variation in the C5 RPI record is an expression of the same geomagnetic feature, although the modest intensity of the feature and the presence of a similar peak with a discrepant age in the Augusta Bay record cast some doubt upon this interpretation.

The inclination record is more complex than the RPI record. Differences between the C5 data and the Augusta Bay curve are more numerous and more pronounced but there is broad agreement of trends at timescales above 100 years. Divergence between the plotted previous records and models is also greater than divergence between the corresponding RPI records. There is a good match between the inclination lows in the Augusta and C5 records at around 3.1–3.0 ka BP, with similar features noticeable in the lower-resolution Tyrrhenian cores ET91-18 and ET95-4. The C5 inclination curve also parallels that of the MP49 core throughout

most of the latter's extent. In the oldest c. 500 years of the record, the C5 inclination data exhibit an upward trend not visible in any of the comparison curves; the results here may have been affected by the tephra layers mentioned above. Throughout the studied interval, the speleothem inclination values recorded by the RMD1 and RMD8 cores are significantly and consistently higher than those of any of the other plotted records, including that of the C5 core – a discrepancy already remarked upon by Zanella *et al.* (2018). In the youngest 400 years of the record, the C5 inclinations are significantly lower than those recorded in the Italian volcanic dataset. The fact that the overall declining trend of the C5 curve parallels that of the volcanic data through most of this interval suggests that the sedimentary data may have been affected by inclination shallowing, which may also explain the shallowness of the C5 curve compared to the Italian archaeomagnetic data throughout much of the 3.0–1.5 ka BP interval.

The declination values remain mostly within the envelope of previously published records, the main exceptions being the last c. 500 years (where C5 declinations are significantly lower than any others) and the interval c. 3.9–3.6 ka BP (where C5 declinations are slightly elevated). In the youngest c. 500 years, the C5 declination record appears to be consistently and negatively offset from the Italian volcanic and archaeomagnetic data (and, therefore, from the SHA.DIF.14k model based on these data). Since, as described in the Methods section, the C5 core sections lack azimuthal orientation, this offset is probably attributable to the empirical method used to reconstruct and realign the declination data. Conversely, in the 3.0–1.5 ka BP interval, the C5 declinations are positively offset from the volcanic and archaeomagnetic declinations. In this case, the data may reflect genuine geographical variations in declination, since the Salerno and Augusta cores also exhibit more positive values within this interval. The declination records of the RMD1 and RMD8 speleothem cores show limited agreement with the C5 core and with the other datasets plotted in the present work, with marked negative outliers both in the 3.5–3.0 and 1.5–0.5 ka BP intervals. Overall, the C5 core shows the best agreement, as might be expected, with the Augusta Bay record; the main discrepancy between the two records is in the interval c. 3.1–2.4 ka BP; in this interval, the Augusta Bay declination swings strongly eastwards (reaching almost 50°), while the C5 record remains in the range 0°–20°, more closely paralleling the other comparison curves. The declination record lacks the 'f' feature described by Turner & Thompson (1981) and identified in Italian records by Vigliotti (2006) at around 3.15 ka BP. This feature is also missing in most of our comparison curves, being clearly expressed

only in the record from the MP49 core of [Béguin et al. \(2019\)](#). Its absence in the C5 core may be attributable to particle realignment from local currents at the coring site.

Overall, there is closer agreement in the RPI curves than in the PSV curves, both between the C5 record and the comparison curves and between the comparison curves themselves.

Discussion of curve-matching results

The experimental age model produced by the curve-matching procedure described in the earlier subsection ‘Evaluation of data’ and shown in [Figure 10](#) does not differ greatly from the linear age model. This is to be expected, given the density of the tie points and their relatively small error margins. Overall, the curve-matched age model is fairly robust: small changes to the parameters supplied to the Match program ([Lisiecki & Lisiecki 2002](#)) have a negligible effect, and even replacing the median RPI curve with the susceptibility-normalized RPI estimate produces an almost identical result. Through most of the older part of the core (*c.* 3.8–1.6 ka BP) the match procedure tends to produce slightly younger ages than the linear age model, suggesting that the palaeomagnetic signal may be affected by lock-in depth in this interval.

The most significant difference between the linear and curve-matched age models is in the *c.* 3.5–3.0 ka BP interval, where the RPI correlation is significantly improved by increasing the inferred sedimentation rate during the younger part of the interval, which moves an RPI trough at *c.* 3.45 ka BP into a much closer alignment with the Augusta Bay record at *c.* 3.25 ka BP. This alignment also reduces the duration of the peak at *c.* 2.95 ka BP, slightly increasing its similarity with published records of the Levantine spike. The effect of this alignment on the PSV records is more difficult to evaluate visually, since there is a greater difference between the measured and reference curves; however, the correlations have not noticeably worsened. Since the initial similarity between the C5 and reference curves was greater for the RPI data than for the PSV data, it is not surprising that the curve-matching procedure has done the most for the RPI record: the restrictions imposed by the tie points mean that only small realignments are possible, and only in the RPI curve can a relatively small realignment be sufficient to improve significantly the correlation between two features.

Conclusions

The C5 record provides a new, high-resolution dataset spanning the past 4.5 kyr in a region for which

relatively little PSV and RPI data have been published. The age control points of [Margaritelli et al. \(2016\)](#) provide an independent age model for our magnetic records, and an automated curve-matching experiment demonstrated that this linear age model differs only very slightly from a tuned age model designed to maximize correlation between our data and reference curves. The data have the potential to be useful in the construction of future Italian and western European master curves, in the improvement of Holocene geomagnetic models, and in the dating of archaeological and volcanic targets, and the rock magnetic data can provide a foundation for future enviromagnetic studies on the same sediments.

Acknowledgements Marine core C5 was collected during oceanographic cruise I-AMICA2013_01. We are grateful to Evdokia Tema, Luigi Vigliotti and an anonymous reviewer for their constructive comments on the manuscript.

Funding This research has been financially supported by the Project of Strategic Interest NextData PNR 2011–13 (<http://www.nextdataproject.it>).

Author contributions **PL:** conceptualization (lead), data curation (lead), formal analysis (lead), investigation (lead), methodology (lead), software (lead), visualization (lead), writing – original draft (lead), writing – review & editing (lead); **FF:** conceptualization (supporting), investigation (supporting), methodology (supporting), project administration (supporting), resources (supporting), supervision (supporting), validation (supporting), writing – original draft (supporting), writing – review & editing (supporting); **SB:** conceptualization (supporting), investigation (supporting), methodology (supporting); **AC:** conceptualization (supporting), investigation (supporting), methodology (supporting); **FDR:** conceptualization (supporting), investigation (supporting), methodology (supporting); **LF:** conceptualization (supporting), investigation (supporting), methodology (supporting), project administration (supporting); **DDI:** conceptualization (supporting), investigation (supporting), methodology (supporting); **DM:** conceptualization (supporting), investigation (supporting), methodology (supporting); **GM:** conceptualization (supporting), investigation (supporting), methodology (supporting); **NP:** conceptualization (supporting), investigation (supporting), methodology (supporting); **PP:** conceptualization (supporting), investigation (supporting), methodology (supporting); **MV:** conceptualization (supporting), investigation (supporting), methodology (supporting); **CC:** conceptualization (supporting), investigation (supporting), methodology (supporting); **FL:** conceptualization (supporting), investigation (supporting), methodology (supporting), project administration (supporting), resources (supporting).

Data availability statement The datasets generated during and/or analysed during the current study are available in the Zenodo repository, <https://doi.org/10.5281/zenodo.1158709>

References

- ARASON, P. & LEVI, S. 2010. Maximum likelihood solution for inclination-only data in paleomagnetism. *Geophysical Journal International*, **182**, 753–771, <https://doi.org/10.1111/j.1365-246X.2010.04671.x>
- ARRIGHI, S., ROSI, M., TANGUY, J.-C. & COURTILLOT, V. 2004. Recent eruptive history of Stromboli (Aeolian Islands, Italy) determined from high-accuracy archaeomagnetic dating. *Geophysical Research Letters*, **31**, L19603, <https://doi.org/10.1029/2004GL020627>
- BARSOTTI, S., NERI, A., BERTAGNINI, A., CIONI, R., MULAS, M. & MUNDULA, F. 2015. Dynamics and tephra dispersal of violent Strombolian eruptions at Vesuvius: insights from field data, wind reconstruction and numerical simulation of the 1906 event. *Bulletin of Volcanology*, **77**, 58, <https://doi.org/10.1007/s00445-015-0939-6>
- BÉGUIN, A., FILIPPIDI, A., DE LANGE, G.J. & DE GROOT, L.V. 2019. The evolution of the Levantine Iron Age geomagnetic Anomaly captured in Mediterranean sediments. *Earth and Planetary Science Letters*, **511**, 55–66, <https://doi.org/10.1016/j.epsl.2019.01.021>
- BEN-YOSEF, E., TAUZE, L., LEVY, T.E., SHAAR, R., RON, H. & NAJJAR, M. 2009. Geomagnetic intensity spike recorded in high resolution slag deposit in Southern Jordan. *Earth and Planetary Science Letters*, **287**, 529–539, <https://doi.org/10.1016/j.epsl.2009.09.001>
- BLUM, P. 1997. *Physical Properties Handbook*. ODP Technical Note, **26**, <https://doi.org/10.2973/odp.tn.26.1997> (retrieved 9 March 2017).
- BONARDI, G., AMORE, F.O., CIAMPO, G., DE CAPOA, P., MICONNET, P. & PERRONE, V. 1988. Il ‘Complesso Liguride’ Auct.: stato delle conoscenze e problemi aperti sulla sua evoluzione pre-appenninica ed i suoi rapporti con l’Arco Calabro. *Memorie della Società Geologica Italiana*, **41**, 17–35
- BONOMO, S., CASCELLA, A. ET AL. 2014. Coccolithophores from near the Volturno estuary (central Tyrrhenian Sea). *Marine Micropaleontology*, **111**, 26–37, <https://doi.org/10.1016/j.marmicro.2014.06.001>
- BONOMO, S., CASCELLA, A. ET AL. 2016. Reworked Coccoliths as runoff proxy for the last 400 years: The case of Gaeta Gulf (central Tyrrhenian Sea, Central Italy). *Palaeogeography, Palaeoclimatology, Palaeoecology*, **459**, 15–28, <https://doi.org/10.1016/j.palaeo.2016.06.037>
- BRENNAN, W.J. 1993. Origin and modification of magnetic fabric in fine-grained detrital sediment by depositional and post-depositional processes. *SEPM Special Publications*, **49**, 17–27.
- BROWN, M., DONADINI, F. ET AL. 2015. GEOMAGIA50.v3: 1. general structure and modifications to the archeological and volcanic database. *Earth, Planets and Space*, **67**, 83, <https://doi.org/10.1186/s40623-015-0232-0>
- BUCUR, I. 1994. The direction of the terrestrial magnetic field in France, during the last 21 centuries. Recent progress. *Physics of the Earth and Planetary Interiors*, **87**, 95–109, [https://doi.org/10.1016/0031-9201\(94\)90024-8](https://doi.org/10.1016/0031-9201(94)90024-8)
- CARICCHI, C., SAGNOTTI, L., CAMPUZANO, S.A., LUCCHI, R.G., MACRÌ, P., REBESCO, M. & CAMERLENGHI, A. 2020. A refined age calibrated paleosecular variation and relative paleointensity stack for the NW Barents Sea: implication for geomagnetic field behavior during the Holocene. *Quaternary Science Reviews*, **229**, 106133, <https://doi.org/10.1016/j.quascirev.2019.106133>
- CASAS, L.I. & INCORONATO, A. 2007. Distribution analysis of errors due to relocation of geomagnetic data using the ‘Conversion via Pole’ (CVP) method: implications on archaeomagnetic data. *Geophysical Journal International*, **169**, 448–454, <https://doi.org/10.1111/j.1365-246X.2007.03346.x>
- CHANNELL, J.E.T., HODELL, D.A. & LEHMAN, B. 1997. Relative geomagnetic paleointensity and $\delta^{18}\text{O}$ at ODP Site 983 (Gardar Drift, North Atlantic) since 350 ka. *Earth and Planetary Science Letters*, **153**, 103–118, [https://doi.org/10.1016/S0012-821X\(97\)00164-7](https://doi.org/10.1016/S0012-821X(97)00164-7)
- CHANNELL, J.E.T., MAZAUD, A., SULLIVAN, P., TURNER, S. & RAYMO, M.E. 2002. Geomagnetic excursions and paleointensities in the Matuyama Chron at Ocean Drilling Program Sites 983 and 984 (Iceland Basin). *Journal of Geophysical Research: Solid Earth*, **107**, EPM1-14, <https://doi.org/10.1029/2001JB000491>
- CHANNELL, J.E.T., HODELL, D.A., CROWHURST, S.J., SKINNER, L.C. & MUSCHELER, R. 2018. Relative paleointensity (RPI) in the latest Pleistocene (10–45 ka) and implications for deglacial atmospheric radiocarbon. *Quaternary Science Reviews*, **191**, 57–72, <https://doi.org/10.1016/j.quascirev.2018.05.007>
- CONSTABLE, C., KORTE, M. & PANOVSKA, S. 2016. Persistent high paleosecular variation activity in southern hemisphere for at least 10 000 years. *Earth and Planetary Science Letters*, **453**, 78–86, <https://doi.org/10.1016/j.epsl.2016.08.015>
- DALY, L. & LE GOFF, M. 1996. An updated and homogeneous world secular variation data base. 1. Smoothing of the archaeomagnetic results. *Physics of the Earth and Planetary Interiors*, **93**, 159–190, [https://doi.org/10.1016/0031-9201\(95\)03075-1](https://doi.org/10.1016/0031-9201(95)03075-1)
- DAVIES, C. & CONSTABLE, C. 2017. Geomagnetic spikes on the core–mantle boundary. *Nature Communications*, **8**, 15593, <https://doi.org/10.1038/ncomms15593>
- DI RITA, F., LIRER, F. ET AL. 2018. Late Holocene forest dynamics in the Gulf of Gaeta (central Mediterranean) in relation to NAO variability and human impact. *Quaternary Science Reviews*, **179**, 137–152, <https://doi.org/10.1016/j.quascirev.2017.11.012>
- FERRARO, L., BONOMO, S. ET AL. 2013. *Rapporto di fine campagna: Campagna Oceanografica I-AMICA_2013_01 progetto PON I-AMICA OR.4.4, Foce del Fiume Volturno, Golfo di Gaeta, Mar Tirreno*, 29 gennaio – 11 febbraio 2013, IAMC–CNR, Naples.
- GALLET, Y., GENEVEY, A. & LE GOFF, M. 2002. Three millennia of directional variation of the Earth’s magnetic field in western Europe as revealed by archaeological artefacts. *Physics of the Earth and Planetary Interiors*, **131**, 81–89, [https://doi.org/10.1016/S0031-9201\(02\)00030-4](https://doi.org/10.1016/S0031-9201(02)00030-4)
- GOEHRING, B.M., MUZIKAR, P. & LIFTON, N.A. 2018. Establishing a Bayesian approach to determining cosmogenic nuclide reference production rates using He-3. *Earth*

- and Planetary Science Letters, **481**, 91–100, <https://doi.org/10.1016/j.epsl.2017.10.025>
- GUYODO, Y., CHANNELL, J.E.T. & THOMAS, R.G. 2002. Deconvolution of u-channel paleomagnetic data near geomagnetic reversals and short events. *Geophysical Research Letters*, **29**, 26-1–26-4, <https://doi.org/10.1029/2002GL014927>
- HARRISON, R.J. & FEINBERG, J.M. 2008. FORCinel: An improved algorithm for calculating first-order reversal curve distributions using locally weighted regression smoothing. *Geochemistry, Geophysics, Geosystems*, **9**, Q05016, <https://doi.org/10.1029/2008GC001987>
- HEIDER, F., DUNLOP, D.J. & SOFFEL, H.C. 1992. Low-temperature and alternating field demagnetization of saturation remanence and thermoremanence in magnetite grains (0.037 µm to 5 mm). *Journal of Geophysical Research: Solid Earth*, **97**, 9371–9381, <https://doi.org/10.1029/91JB03097>
- HERNANDEZ-QUINTERO, E., GOGUITCHAICHVILI, A., CEJUDO, R., CIFUENTES, G., GARCIA, R. & CERVANTES, M. 2020. Spatial distribution of historical geomagnetic measurements in Mexico. *Journal of South American Earth Sciences*, **100**, 102556, <https://doi.org/10.1016/j.jsames.2020.102556>
- HESLOP, D., DEKKERS, M.J., KUIVER, P.P. & VAN OORSCHOT, I.H.M. 2002. Analysis of isothermal remanent magnetization acquisition curves using the expectation–maximization algorithm. *Geophysical Journal International*, **148**, 58–64, <https://doi.org/10.1046/j.0956-540x.2001.01558.x>
- IERMANO, I., LIGUORI, G. ET AL. 2012. Filament formation and evolution in buoyant coastal waters: observation and modelling. *Progress in Oceanography*, **106**, 118–137, <https://doi.org/10.1016/j.pocean.2012.08.003>
- IORIO, M., LIDDICOAT, J.C., BUDILLON, F., TIANO, P., INCORONATO, A., COE, R.S. & MARSELLA, E. 2009. Paleomagnetic secular variation time constraints on Late Neogene geological events in slope sediment from the eastern Tyrrhenian sea. *SEPM Special Publications*, **92**, 233–243.
- JOHNSON, C.L., WIJBRANS, J.R. ET AL. 1998. $^{40}\text{Ar}/^{39}\text{Ar}$ ages and paleomagnetism of São Miguel lavas, Azores. *Earth and Planetary Science Letters*, **160**, 637–649, [https://doi.org/10.1016/S0012-821X\(98\)00117-4](https://doi.org/10.1016/S0012-821X(98)00117-4)
- KIRSCHVINK, J.L. 1980. The least-squares line and plane and the analysis of palaeomagnetic data. *Geophysical Journal of the Royal Astronomical Society*, **62**, 699–718, <https://doi.org/10.1111/j.1365-246X.1980.tb02601.x>
- KODAMA, K.P. 2012. *Paleomagnetism of Sedimentary Rocks: Process and Interpretation*. Wiley-Blackwell, Chichester, UK.
- KORTE, M. & CONSTABLE, C.G. 2018. Archeomagnetic intensity spikes: global or regional geomagnetic field features? *Frontiers in Earth Science*, **6**, 17, <https://doi.org/10.3389/feart.2018.00017>
- LIRER, F., SPROVIERI, M. ET AL. 2013. Integrated stratigraphy for the Late Quaternary in the eastern Tyrrhenian Sea. *Quaternary International*, **292**, 71–85, <https://doi.org/10.1016/j.quaint.2012.08.2055>
- LIRER, F., SPROVIERI, M., VALLEFUOCO, M., FERRARO, L., PELOSI, N., GIORDANO, L. & CAPOTONDI, L. 2014. Planktonic foraminifera as bio-indicators for monitoring the climatic changes that have occurred over the past 2000 years in the southeastern Tyrrhenian Sea. *Integrative Zoology*, **9**, 542–554, <https://doi.org/10.1111/1749-4877.12083>
- LISIECKI, L.E. & LISIECKI, P.A. 2002. Application of dynamic programming to the correlation of paleoclimate records. *Paleoceanography*, **17**, 1049, <https://doi.org/10.1029/2001PA000733>
- LUND, S., PLATZMAN, E. & JOHNSON, T.C. 2020. Paleomagnetic secular variation records from Holocene sediments of Lake Victoria (0.5°S, 33.3°E). *The Holocene*, <https://doi.org/10.1177/0959683619901214>
- LURCOCK, P.C. & FLORINDO, F. 2019. New developments in the PuffinPlot paleomagnetic data analysis program. *Geochemistry, Geophysics, Geosystems*, **20**, 5578–5587, <https://doi.org/10.1029/2019GC008537>
- LURCOCK, P.C. & WILSON, G.S. 2012. Puffinplot: a versatile, user-friendly program for paleomagnetic analysis. *Geochemistry, Geophysics, Geosystems*, **13**, Q06Z45, <https://doi.org/10.1029/2012GC004098>
- MARGARIELLI, G., VALLEFUOCO, M. ET AL. 2016. Marine response to climate changes during the last four millennia in the central Mediterranean Sea. *Global and Planetary Change*, **142**, 53–72, <https://doi.org/10.1016/j.gloplacha.2016.04.007>
- MASTROLorenzo, G., MUNNO, R. & ROLANDI, G. 1993. Vesuvius 1906: a case study of a paroxysmal eruption and its relation to eruption cycles. *Journal of Volcanology and Geothermal Research*, **58**, 217–237, [https://doi.org/10.1016/0377-0273\(93\)90110-D](https://doi.org/10.1016/0377-0273(93)90110-D)
- MCELHINNY, M.W. & McFADDEN, P.L. 2000. *Paleomagnetism: Continents and Oceans*. Academic Press, San Diego, CA.
- NILSSON, A., HOLME, R., KORTE, M., SUTTIE, N. & HILL, M. 2014. Reconstructing Holocene geomagnetic field variation: new methods, models and implications. *Geophysical Journal International*, **198**, 229, <https://doi.org/10.1093/gji/ggu120>
- NOEL, M. & BATTI, C.M. 1990. A method for correcting geographically separated remanence directions for the purpose of archaeomagnetic dating. *Geophysical Journal International*, **102**, 753–756, <https://doi.org/10.1111/j.1365-246X.1990.tb04594.x>
- PANOVSKA, S., KORTE, M. & CONSTABLE, C.G. 2019. One hundred thousand years of geomagnetic field evolution. *Reviews of Geophysics*, **57**, 1289–1337, <https://doi.org/10.1029/2019RG000656>
- PAVÓN-CARRASCO, F.J., OSSETE, M.L., TORTA, J.M. & SANTIS, A.D. 2014. A geomagnetic field model for the Holocene based on archaeomagnetic and lava flow data. *Earth and Planetary Science Letters*, **388**, 98–109, <https://doi.org/10.1016/j.epsl.2013.11.046>
- PETERS, C. & DEKKERS, M.J. 2003. Selected room temperature magnetic parameters as a function of mineralogy, concentration and grain size. *Physics and Chemistry of the Earth, Parts A/B/C*, **28**, 659–667, [https://doi.org/10.1016/S1474-7065\(03\)00120-7](https://doi.org/10.1016/S1474-7065(03)00120-7)
- PETROVSKÝ, E. & KAPIČKA, A. 2006. On determination of the Curie point from thermomagnetic curves. *Journal of Geophysical Research: Solid Earth*, **111**, B12S27, <https://doi.org/10.1029/2006JB004507>
- PIKE, C.R., ROBERTS, A.P. & VEROB, K.L. 1999. Characterizing interactions in fine magnetic particle systems using first order reversal curves. *Journal of Applied Physics*, **85**, 6660–6667, <https://doi.org/10.1063/1.370176>

- ROBERTS, A.P., PIKE, C.R. & VEROUB, K.L. 2000. First-order reversal curve diagrams: A new tool for characterizing the magnetic properties of natural samples. *Journal of Geophysical Research: Solid Earth*, **105**, 28 461–28 475, <https://doi.org/10.1029/2000JB900326>
- ROBERTS, A.P., HESLOP, D., ZHAO, X. & PIKE, C.R. 2014. Understanding fine magnetic particle systems through use of first-order reversal curve diagrams. *Reviews of Geophysics*, **52**, 557–602, <https://doi.org/10.1002/2014RG000462>
- ROBERTSON, D.J. & FRANCE, D.E. 1994. Discrimination of remanence-carrying minerals in mixtures, using isothermal remanent magnetisation acquisition curves. *Physics of the Earth and Planetary Interiors*, **82**, 223–234, [https://doi.org/10.1016/0031-9201\(94\)90074-4](https://doi.org/10.1016/0031-9201(94)90074-4)
- SAGNOTTI, L., SMEDILE, A. ET AL. 2011. A continuous palaeosecular variation record of the last four millennia from the Augusta Bay (Sicily, Italy). *Geophysical Journal International*, **184**, 191–202, <https://doi.org/10.1111/j.1365-246X.2010.04860.x>
- SÁNCHEZ-MORENO, E.M., CALVO-RATHERT, M., GOUGITCH-AICHVILI, A., TAUZE, L., VASHAKIDZE, G.T. & LEBEDEV, V.A. 2020. Weak palaeointensity results over a Pliocene volcanic sequence from Lesser Caucasus (Georgia): transitional record or time averaged field? *Geophysical Journal International*, **220**, 1604–1618, <https://doi.org/10.1093/gji/ggz533>
- SHAAR, R., BEN-YOSEF, E., RON, H., TAUZE, L., AGNON, A. & KESSEL, R. 2011. Geomagnetic field intensity: How high can it get? How fast can it change? Constraints from Iron Age copper slag. *Earth and Planetary Science Letters*, **301**, 297–306, <https://doi.org/10.1016/j.epsl.2010.11.013>
- SHAAR, R., TAUZE, L., RON, H., EBERT, Y., ZUCKERMAN, S., FINKELSTEIN, I. & AGNON, A. 2016. Large geomagnetic field anomalies revealed in Bronze to Iron Age archeomagnetic data from Tel Megiddo and Tel Hazor, Israel. *Earth and Planetary Science Letters*, **442**, 173–185, <https://doi.org/10.1016/j.epsl.2016.02.038>
- SHAAR, R., HASSUL, E. ET AL. 2018. The first catalog of archeomagnetic directions from Israel with 4000 years of geomagnetic secular variations. *Frontiers in Earth Science*, **6**, 164, <https://doi.org/10.3389/feart.2018.00164>
- SMITH, V.C., ISAIA, R. & PEARCE, N.J.G. 2011. Tephrostratigraphy and glass compositions of post-15 kyr Campi Flegrei eruptions: implications for eruption history and chronostratigraphic markers. *Quaternary Science Reviews*, **30**, 3638–3660, <https://doi.org/10.1016/j.quascirev.2011.07.012>
- SUPERANZA, F., BRANCA, S., COLTELLI, M., D'AJELLO CARACCIOLI, F. & VIGLIOTTI, L. 2006. How accurate is ‘paleomagnetic dating’? New evidence from historical lavas from Mount Etna. *Journal of Geophysical Research: Solid Earth*, **111**, B12S33, <https://doi.org/10.1029/2006JB004496>
- TAUXE, L. 1993. Sedimentary records of relative paleointensity of the geomagnetic field: theory and practice. *Reviews of Geophysics*, **31**, 319–354, <https://doi.org/10.1029/93RG01771>
- TEMA, E., HEDLEY, I. & LANOS, P. 2006. Archaeomagnetism in Italy: a compilation of data including new results and a preliminary Italian secular variation curve. *Geophysical Journal International*, **167**, 1160–1171, <https://doi.org/10.1111/j.1365-246X.2006.03150.x>
- TURNER, G.M. & THOMPSON, R. 1981. Lake sediment record of the geomagnetic secular variation in Britain during Holocene times. *Geophysical Journal International*, **65**, 703–725, <https://doi.org/10.1111/j.1365-246X.1981.tb04879.x>
- TURNER, G.M., KINGER, R., MCFADGEN, B. & GEVERS, M. 2020. The first archaeointensity records from New Zealand: evidence for a fifteenth century AD archaeomagnetic ‘spike’ in the SW Pacific region? *Geological Society, London, Special Publications*, **497**, <https://doi.org/10.1144/SP497-2019-71>
- VIGLIOTTI, L. 2006. Secular variation record of the Earth's magnetic field in Italy during the Holocene: constraints for the construction of a master curve. *Geophysical Journal International*, **165**, 414–429, <https://doi.org/10.1111/j.1365-246X.2005.02785.x>
- VIGLIOTTI, L., VEROUB, K., CATTANEO, A., TRINCARDI, F., ASIOLI, A. & PIVA, A. 2008. Palaeomagnetic and rock magnetic analysis of Holocene deposits from the Adriatic Sea: detecting and dating short-term fluctuations in sediment supply. *The Holocene*, **18**, 141–152, <https://doi.org/10.1177/0959683607085605>
- XUAN, C. & CHANNELL, J.E.T. 2009. UPmag: MATLAB software for viewing and processing u channel or other pass-through paleomagnetic data. *Geochemistry, Geophysics, Geosystems*, **10**, Q10Y07, <https://doi.org/10.1029/2009GC002584>
- ZANELLA, E., TEMA, E. ET AL. 2018. A 10 000 yr record of high-resolution paleosecular variation from a flowstone of Rio Martino Cave, northwestern Alps, Italy. *Earth and Planetary Science Letters*, **485**, 32–42, <https://doi.org/10.1016/j.epsl.2017.12.047>
- ZIDERVERD, J.D.A. 1967. A. C. demagnetization of rocks: analysis of results. *Developments in Solid Earth Geophysics*, **3**, 254–286, <https://doi.org/10.1016/B978-1-4832-2894-5.50049-5>